computed at Mach 3.5 and 3.0 at a wind-tunnel Reynolds number of $4.5 \times 10^6$/ft and zero angle of attack. The computed flow features were consistent with the prior computations of Ref. 2. The new boattail and fin boom flow indicated that the vortex sheet (surface) extended over the boattail, thus inhibiting the usual wave expansion fan expected at the body–boattail junction.

2) The flow over the cone-nosed body of the M830A1 projectile with the 12.5- and 4.5-deg biboattails (configuration 2) was computed for Mach 4.3, 3.95, and 2.05 at sea-level Reynolds numbers of 30.1, 27.6, and $14.3 \times 10^6$/ft, respectively. The flow showed very small flow unsteadiness at the nose meplat at Mach 4.3, and it disappeared at Mach 2.05. There were evident expansion waves at the body–boattail junction due to the absence of the vortex sheet of a vortex ring.

3) The 40%-scaled-down model, a cone-nosed configuration of 20.5- and 4.6-deg biboattails (configuration 3), was computed at wind-tunnel Reynolds numbers of $9.1 \times 10^6$ and $10.2 \times 10^6$/ft for Mach 3.5 and 3.0, respectively. The axial force coefficient was compared with data, and indicated good agreement at Mach 3 and a measurement error at Mach 3.5, where the measured value increased rather than decreased, in contradiction of the normal trend.

4) The drag-component anatomy was examined for all cases computed. For the spiked cases, the spike tip and body shoulder contributed 25 and 60% of the total drag at $M = 3$. For the coned configuration (configuration 3), the nose and boattails contributed 57 and 32%, respectively, at Mach 3. No experiment, yet, has provided such an insight into the drag anatomy.

5) Contrary to the general expectation, the spike-nosed configuration drag was not much higher than the cone-nosed drag in the Mach 3.0–3.5 range. This finding is limited to spiked bodies with vortex generator rings, at the low-drag mode, at Mach $\geq$3.0. A spiked body without the ring can suffer much higher drag than the cone-nosed body at lower speeds ($M < 3$), especially in the spike high-drag mode.

6) The present computations indicated that these two classes of configurations can be successfully computed with the presented approach. This work, therefore, paves the way to computing the complete projectile configuration by including the fins.

## References

[1]Mikhail, A. G., "Spiked-Nosed Projectiles: Computations and Dual Flow Modes in Supersonic Flight," *Journal of Spacecraft and Rockets*, Vol. 28, No. 4, 1991, pp. 418–424; AIAA Paper 89-1820.

[2]Mikhail, A. G., "Spike-Nosed Projectiles with Vortex Rings: Steady and Unsteady Flow Simulations," AIAA Paper 91-3261, Sept. 1991.

[3]Patel, N. R., and Sturek, W. B., "Multi-Tasked Numerical Simulation of Axisymmetric Ramjet Flows Using Zonal Overlapped Grids," U.S. Army Ballistic Research Lab., BRL-MR-3834, Aberdeen Proving Ground, MD, May 1990.

[4]Falkowski, E. W., "Static and Dynamic Stability Characteristics of the Supersonic Infantry Projectile at Transonic Velocities," U.S. Army Picatinny Arsenal, TM-1565, Dover, NJ, June 1965.

[5]Biele, J. K., "Drag and Flow Field Characteristics of Two Complex-Shaped Projectile Types," *Proceedings of the 7th International Symposium on Ballistics* (The Hague, The Netherlands), American Defence Preparedness Association, 1983, pp. 221–229.

[6]Farina, T., and Choudhary, A., "Wind Tunnel Test Results of an Advanced Multipurpose Tank Fired Projectile," U.S. Army Armament Research, Development and Engineering Center, ARDEC-TR-91015, Picatinny Arsenal, NJ, Oct. 1991.

[7]Mikhail, A. G., "Flow Simulation and Drag Anatomy for Anti-Tank Projectile Configurations," AIAA Paper 94-0153, Jan. 1994.

[8]Haupt, B. F., Buff, R. S., and Koening, K., "Aerodynamic Effects of Probe-Induced Flow Separation on Bluff Bodies at Transonic Mach Numbers," AIAA Paper 85-0103, Jan. 1985.

[9]Calarese, W., and Hankey, W. L., "Modes of Shock Wave Oscillations on Spike-Tipped Bodies," *AIAA Journal*, Vol. 23, No. 2, 1985, pp. 185–192.

[10]Shang, J. S., Hankey, W. L., and Smith, R. E., "Flow Oscillations of Spike-Tipped Bodies," *AIAA Journal*, Vol. 20, No. 1, 1982, pp. 25, 26.

[11]Mikhail, A. G., "Data Correlation and Surface Groove Drag for Kinetic Energy Projectiles," *Journal of Spacecraft and Rockets*, Vol. 26, No. 5, 1989, pp. 308–313; AIAA Paper 88–2541.

J. Allen
*Associate Editor*

# Engineering Interactive Inviscid Boundary-Layer Method for Hypersonic Flow

Christopher J. Riley*
*NASA Langley Research Center, Hampton, Virginia 23681*
and
Fred R. DeJarnette†
*North Carolina State University, Raleigh, North Carolina 27695*

## Introduction

ENGINEERING inviscid boundary layer methods[1–4] have been demonstrated to adequately predict the convective heating over a wide range of hypersonic vehicle geometries and aerothermal environments. Various approximations in the inviscid and boundary-layer regions enable a solution to be generated in a fraction of the time required by Navier–Stokes (NS), parabolized Navier–Stokes (PNS), viscous shock layer (VSL), or complete Euler/boundary-layer solvers. This reduction in computer time makes the engineering aerothermal methods ideal for parametric studies.

Although much effort has gone into developing coupled Euler/boundary layer codes[5–9] that allow interaction between the inviscid and viscous regions, the existing engineering methods follow a classical boundary-layer analysis. The inviscid flowfield influences the boundary-layer solution, but the viscous layer is assumed to have a negligible effect on the outer inviscid region. This assumption is accurate for relatively high Reynolds number flows where the boundary layer is thin compared to the shock layer. At lower Reynolds numbers, the thicker boundary layer displaces the outer flow and increases the surface pressure and heat transfer. Neglecting this displacement effect at lower Reynolds numbers may lead to inaccurate results.

To improve the capability of the engineering methods for lower Reynolds number flows, a current engineering aerothermal method has been modified to include the effects of viscous interaction. This algorithm is referred to as three-dimensional hypersonic inviscid boundary-layer method (THINBL).[10,11] It includes a simplified inviscid technique based on thin shock-layer theory for computing the three-dimensional outer flow,[12,13] a method of computing surface streamlines that allows the use of any axisymmetric boundary-layer technique for the viscous solution, and a set of approximate convective heating equations.[14] This Note outlines the viscous interaction procedure used in THINBL and demonstrates its effect on a spherically blunted cone at a representative low Reynolds number condition.

## Analysis

This section briefly describes the engineering inviscid boundary-layer method THINBL. An outline of the viscous interaction procedure is also given. More details may be found in Refs. 10–13.

### THINBL

The three-dimensional inviscid analysis[12,13] used in THINBL is simplified by using approximate stream functions in the shock layer and by using an explicit expression for the pressure across the shock

Received May 30, 1995; revision received July 28, 1995; accepted for publication Aug. 1, 1995. 

*Aerospace Engineer, Aerothermodynamics Branch, Gas Dynamics Division. Member AIAA.

†Professor, Mechanical and Aerospace Engineering Department. Associate Fellow AIAA.

layer. In the subsonic blunt-nose region, the shock shape is iteratively varied until the correct body shape is obtained. Beyond this region, the shock surface is determined using a marching technique. This three-dimensional inviscid method has been applied to spherically blunted cones, paraboloids, and blunted cones with elliptical cross sections at angle of attack.

The three-dimensional boundary-layer analysis[10,11] is simplified by using the axisymmetric analog[15] approximation as is done in most engineering aerothermal methods. This approximation allows axisymmetric boundary-layer methods to be employed along an inviscid surface streamline. Streamlines are determined by solving the inviscid momentum equations along the body surface using the body geometry and the surface pressure distribution generated by the approximate three-dimensional inviscid method. In lieu of numerically integrating the boundary-layer equations, a set of approximate convective heating equations developed by Zoby et al.[14] is used for the viscous solution. These relations are valid for laminar and turbulent, perfect gas or equilibrium air flows. Boundary-layer edge properties are found by interpolating in the approximate inviscid solution a distance away from the wall equal to the boundary-layer thickness. Predicted surface heating rates have been shown to compare favorably with numerical solutions of the NS and VSL equations for both axisymmetric and three-dimensional body shapes at angle of attack at relatively high Reynolds number conditions.

### Viscous Interaction

Viscous interaction is included in THINBL by modifying the boundary condition in the inviscid method. An effective body shape is created by adding the displacement thickness of the boundary layer $\delta^*$ to the actual body shape as shown in Fig. 1. The inviscid solution is then recalculated over the effective body shape. A new displacement thickness is computed since the inviscid properties have now changed, and the process is repeated until convergence (typically 3–4 iterations). Thus, the inviscid region is displaced from the true body surface a distance equal to $\delta^*$.

For laminar flow, expressions for the boundary-layer and displacement thicknesses are found in Ref. 16 and are given by

$$\delta/\theta = 5.55 + u_e^2/2h_e \tag{1}$$

and

$$\delta^*/\theta = u_e^2/2h_e \tag{2}$$

where $\delta$ and $\theta$ represent the boundary-layer and momentum thicknesses, respectively. The velocity and enthalpy at the edge of the boundary layer are given by $u_e$ and $h_e$. The constant 5.55 in Eq. (1) is identical to the one used by Zoby et al.[14] and is valid for a cold wall and arbitrary pressure gradient in the analysis of Ref. 16. The other term in Eqs. (1) and (2), $u_e^2/2h_e$, corresponds to a cold wall and zero pressure gradient (flat plate). The corresponding turbulent thicknesses are obtained from Ref. 17 as

$$\frac{\delta}{\theta} = N + 1 + \left[\left(\frac{N+2}{N}\frac{h_w}{h_{aw}} + 1\right)\left(1 + 1.29 Pr_w^{\frac{1}{3}} \frac{u_e^2}{2h_e}\right)\right] \tag{3}$$

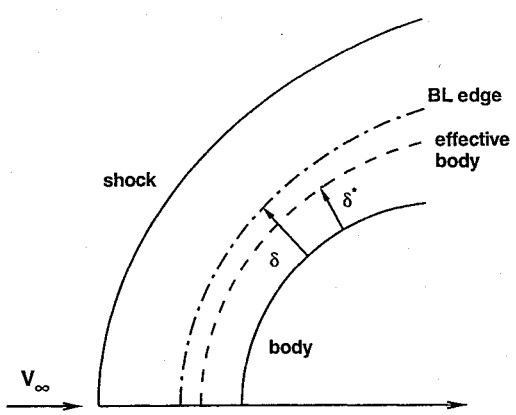


Fig. 1 Boundary-layer displacement thickness.

and

$$\frac{\delta^*}{\theta} = -1 + \left[\left(\frac{N+2}{N}\frac{h_w}{h_{aw}} + 1\right)\left(1 + 0.97 Pr_w^{\frac{1}{3}} \frac{u_e^2}{2h_e}\right)\right] \tag{4}$$

where $h_w$ and $h_{aw}$ represent the wall and adiabatic-wall enthalpies and $N$ is computed from a curve fit[14] of axisymmetric nozzle wall data as

$$N = 12.67 - 6.5\log(Re_\theta) + 1.21[\log(Re_\theta)]^2 \tag{5}$$

The expression for $\delta$ is the same one used by Zoby et al.[14] For both laminar and turbulent flows, boundary-layer edge properties are now obtained by interpolating in the inviscid solution a distance away from the effective body surface equal to $\delta - \delta^*$. Note that the inviscid region now extends only from the shock to the effective body, which is displaced from the true body surface.

## Results and Discussion

To assess the effect of including viscous interaction in the THINBL code, results are presented for a 5-deg spherically blunted cone with a nose radius of 0.0254 m (1 in.) at a low-freestream Reynolds number of 2722 based on nose radius. Freestream conditions correspond to Mach 20 flight at an altitude of 60.96 km (200,000 ft) at 0-deg angle of attack. The flow is assumed to be a perfect gas and laminar, although the modifications to the THINBL method are also applicable to equilibrium air or turbulent flow. The wall temperature is 300 K. Using a VSL method, Lee et al.[18] determined that low-density effects such as shock and body slip are insignificant at these conditions. Results from the THINBL code, both including and neglecting viscous interaction, are compared with a solution generated by the thin-layer NS code LAURA.[19] The LAURA solution is computed using a 200 × 80 grid.

Figures 2 and 3 highlight the effect of the viscous interaction on surface pressures and heat transfer. The displacement effect of the boundary layer causes a rise in both surface quantities. As shown in Figs. 2 and 3, the largest increase is in the vicinity of the pressure minimum ($x/R_n \approx 40$), where the inclusion of viscous interaction in THINBL increases the pressure and heating by 35 and 17%, respectively. Comparisons with computed results from LAURA show agreement within 10% in this region. Farther downstream, the increase in surface quantities is much less. This is expected since in the weak interaction region downstream, the displacement thickness grows gradually and only weakly affects the inviscid flowfield. The corresponding changes in the outer inviscid flow have a negligible effect on the boundary layer and the surface heating. Therefore, the stronger interaction effects are seen in the blunt-nose dominated region. Note that these results depend strongly on the freestream Reynolds number. Increasing the Reynolds number by moving down in altitude or by increasing the nose radius of the sphere cone will reduce the extent of the viscous interaction region. Conversely, decreasing the Reynolds number by moving to a higher

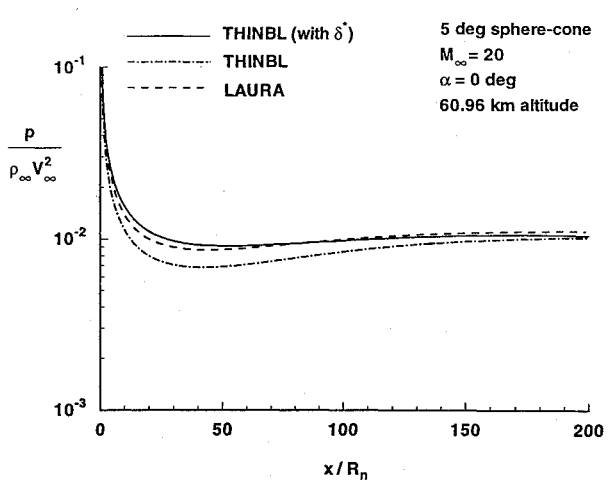


Fig. 2 Viscous interaction effect on surface pressure.

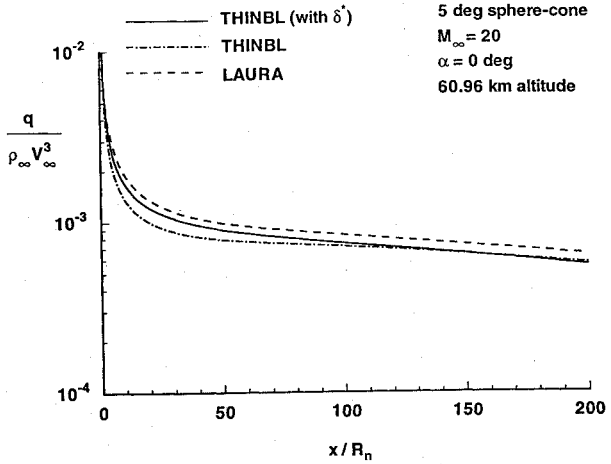


**Fig. 3 Viscous interaction effect on surface heating rates.**

altitude or by decreasing the nose radius will extend the interaction effects downstream.

## Concluding Remarks

An existing engineering inviscid boundary-layer method has been modified to allow the inviscid and boundary-layer regions to interact. Simple expressions for the boundary-layer and displacement thicknesses are presented and are consistent with the approximate convective heating equations used in the code. The effect of viscous interaction on surface pressure and heat transfer is examined for a spherically blunted cone at a low Reynolds number. Including viscous interaction results in improved surface pressure and heating comparisons with predicted quantities from a thin-layer NS method. Allowing for the displacement effect of the boundary layer is a simple and effective means of extending the capabilities of engineering aerothermal methods to include moderate and low Reynolds number flows.

## References

[1]DeJarnette, F. R., and Hamilton, H. H., "Inviscid Surface Streamlines and Heat Transfer on Shuttle-Type Configurations," *Journal of Spacecraft and Rockets*, Vol. 10, No. 5, 1973, pp. 314–321.

[2]DeJarnette, F. R., and Hamilton, H. H., "Aerodynamic Heating on 3-D Bodies Including the Effects of Entropy-Layer Swallowing," *Journal of Spacecraft and Rockets*, Vol. 12, No. 1, 1975, pp. 5–12.

[3]Zoby, E. V., and Simmonds, A. L., "Engineering Flowfield Method with Angle-of-Attack Applications," *Journal of Spacecraft and Rockets*, Vol. 22, No. 4, 1985, pp. 398–405.

[4]Hamilton, H. H., DeJarnette, F. R., and Weilmuenster, K. J., "Application of Axisymmetric Analog for Calculating Heating in Three-Dimensional Flows," *Journal of Spacecraft and Rockets*, Vol. 24, No. 4, 1987, pp. 296–302.

[5]Aupoix, B., Brazier, J. P., and Cousteix, J., "Asymptotic Defect Boundary-Layer Theory Applied to Hypersonic Flow," *AIAA Journal*, Vol. 30, No. 5, 1992, pp. 1252–1259.

[6]Hall, D. W., Hines, R. W., Baltakis, F. P., and Wardlaw, A. B., "Coupled Inviscid/Viscous Aerodynamic Predictions for Supersonic Tactical Missiles," AIAA Paper 90-0617, Jan. 1990.

[7]Monnoyer, F., Mundt, C., and Pfitzner, M., "Calculation of the Hypersonic Viscous Flow Past Reentry Vehicles with an Euler-Boundary Layer Coupling Method," AIAA Paper 90-0417, Jan. 1990.

[8]Wuthrich, S., and Sawley, M. L., "Coupled Euler/Boundary-Layer Method for Nonequilibrium Chemically Reacting Hypersonic Flows," *AIAA Journal*, Vol. 30, No. 12, 1992, pp. 2836–2844.

[9]DeJarnette, F. R., and Radcliffe, R. A., "Matching Inviscid/Boundary Layer Flowfields," AIAA Paper 94-0128, Jan. 1994.

[10]Riley, C. J., and DeJarnette, F. R., "Engineering Aerodynamic Heating Method for Hypersonic Flow," *Journal of Spacecraft and Rockets*, Vol. 29, No. 3, 1992, pp. 327–334.

[11]Riley, C. J., "An Engineering Method for Interactive Inviscid-Boundary Layers in Three-Dimensional Hypersonic Flow," Ph.D. Thesis, Dept. of Mechanical and Aerospace Engineering, North Carolina State Univ., Raleigh, NC, May 1992.

[12]Riley, C. J., and DeJarnette, F. R., "An Approximate Method for Calculating Three-Dimensional Inviscid Hypersonic Flow Fields," NASA TP-3018, Aug. 1990.

[13]Riley, C. J., and DeJarnette, F. R., "Engineering Calculations of Three-Dimensional Inviscid Hypersonic Flow Fields," *Journal of Spacecraft and Rockets*, Vol. 28, No. 6, 1991, pp. 628–635.

[14]Zoby, E. V., Moss, J. N., and Sutton, K., "Approximate Convective-Heating Equations for Hypersonic Flows," *Journal of Spacecraft and Rockets*, Vol. 18, No. 1, 1981, pp. 64–70.

[15]Cooke, J. C., "An Axially Symmetric Analogue for General Three-Dimensional Boundary Layers," British Ministry of Aviation, Aeronautical Research Council TR R&M 3200, June 1961.

[16]Cohen, C. B., and Reshotko, E., "The Compressible Laminar Boundary Layer with Heat Transfer and Arbitrary Pressure Gradient," NACA Rept. 1294, 1956.

[17]Walker, G. K., and Schumann, B. A., "The Growth of Turbulent Boundary Layers," General Electric Co., TIS No. R61SD123, July 1961.

[18]Lee, K. P., Gupta, R. N., Zoby, E. V., and Moss, J. N., "Hypersonic Viscous Shock-Layer Solutions Over Long Slender Bodies II: Low Reynolds Number Flows," *Journal of Spacecraft and Rockets*, Vol. 27, No. 2, 1990, pp. 185–193.

[19]Gnoffo, P. A., "An Upwind-Biased, Point-Implicit Relaxation Algorithm for Viscous, Compressible Perfect-Gas Flows," NASA TP-2953, Feb. 1990.

J. C. Adams
*Associate Editor*